# Bayesian Inference-Based Estimation of Hourly Primary and Secondary Organic Carbon at Suburban Hong Kong: Multi-temporal Scale Variations and Evolution Characteristics during PM2.5 episodes

5    Shan Wang[1#], Kezheng Liao[2#], Zijing Zhang[1], Yuk Ying Cheng[2], Qiongqiong Wang[3, 2], Hanzhe Chen[1], and Jian Zhen Yu[1,2,*]

[1]Division of Environment and Sustainability, The Hong Kong University of Science and Technology, Clear Water Bay, Hong Kong, China

[2]Department of Chemistry, The Hong Kong University of Science and Technology, Clear Water Bay, Hong Kong,
10    China

[3]School of Environmental Studies, China University of Geosciences, Wuhan, China

[#]These authors contributed equally to this work.

*Corresponding to: Jian Zhen Yu (jian.yu@ust.hk)

**Abstract.** Observation-based data of primary and secondary organic carbon in ambient particulate matter (PM) are
15    essential for model evaluation, climate and air quality research, health effects assessment, and mitigation policy development. Since there are no direct measurement tools available to quantify primary organic (POC) and secondary organic carbon (SOC) as separate quantities, their estimation relies on inference approaches using relevant measurable PM constituents. In this study, we measured hourly carbonaceous components and major ions in PM2.5 for a year and a half in suburban Hong Kong from July 2020 to December 2021. We differentiated POC and SOC using a novel
20    Bayesian inference approach, with sulfate identified as the most suitable SOC tracer. The hourly POC and SOC data allowed us to examine temporal characteristics varying from diurnal and weekly patterns to seasonal variations, as well as their evolution characteristics during individual PM2.5 episodes. A total of 65 city-wide PM2.5 episodes were identified throughout the entire studied period, with SOC contributions during individual episodes varying from 10% to 66%. In summertime typhoon episodes, elevated SOC levels were observed during daytime hours, and high
25    temperature and $NO_x$ levels were identified as significant factors contributing to episodic SOC formation. Winter haze episodes exhibited high SOC levels, likely due to persistent influences from regional transport originating from the northern region to the sampling site. Enhanced SOC formation was observed with the increase in nocturnal $NO_3$ radical (represented by $[NO_2][O_3]$) under conditions of high water content and strong acidity. This suggests that aqueous-phase reactions involving $NO_3$ radical were likely a notable contributor to SOC formation during winter haze episodes.
30    The methodology employed in this study for estimating POC and SOC provides practical guidance for other locations with similar monitoring capabilities in place. The availability of hourly POC and SOC data is invaluable for evaluating and improving atmospheric models, as well as understanding the evolution processes of PM pollution episodes. This, in turn, leads to more accurate model predictions and a better understanding of the contributing sources and processes.

## 1 Introduction

35   Carbonaceous aerosol is a major component of PM$_{2.5}$ (particulate matter with an aerodynamic diameter of less than 2.5 μm), accounting for 20-90% of its total mass in ambient environment (Kroll et al., 2011; Seinfeld and Pandis, 1998). It has been known to have adverse effects on regional to global climate, air quality, and human health (Bond et al., 2013; Huang et al., 2014; Nel, 2005). Carbonaceous components can generally be classified into elemental carbon (EC) and organic carbon (OC). EC refers to the soot-like amorphous carbon emitted directly from incomplete

40   combustion processes (Chow et al., 2010), while OC is a more complex mixture of organic compounds which can be either primarily emitted from anthropogenic sources (e.g., biomass burning, fossil fuel combustion, and cooking) and biogenic sources (e.g., plant debris), or secondarily formed through oxidation reactions (Christian et al., 2003; Donahue et al., 2009; Hallquist et al., 2009; Zhao et al., 2007). Therefore, OC can be further group to primary OC (POC) and secondary OC (SOC). Accurately quantifying and estimating POC and SOC through observation-based

45   measurement is the precondition for comprehending their unique characteristics, such as relative contributions, temporal variations, and chemical evolution. This knowledge is crucial for refining atmospheric models and developing more targeted strategies to reduce carbonaceous aerosol emissions, mitigate climate change, and minimize human exposure.

The thermal-optical protocols have been widely used for OC and EC measurements (Chow et al., 2001; Klingshirn et

50   al., 2019). However, accurately determining POC and SOC remains challenging since there are no instrument tools available for the direct measurement of POC and SOC. Several data treatment methodologies have been developed to estimate POC and SOC levels. One such approach is the chemical mass balance (CMB) receptor model, which apportions POC based on the chemical profile of individual known primary sources and the unmapped mass is then referred to as SOC (Pachon et al., 2010; Schauer and Cass, 2000; Shi et al., 2011). However, the uncertainty is large

55   due to limited or insufficient information on the SOC source profiles in CMB simulations (Stone et al., 2009). Another widely used receptor model, positive matrix factorization (PMF), apportions the sources of OC based on the comprehensive chemical speciation data (Jaeckels et al., 2007; Ke et al., 2008). Studies have shown that PMF model output may underestimate the contributions of secondary organic aerosols when the specific molecular organic tracers are absent in the input data matrix (Pachon et al., 2010; Wang et al., 2017). These limitations compromise the

60   applicability of receptor models in accurately quantifying the POC and SOC mass. Alternative approaches include the EC tracer method, which relies on the EC-to-OC ratio (Day et al., 2015; Turpin and Huntzicker, 1991), and the multiple linear regression (MLR) model (Blanchard et al., 2008). The former assumes that POC and EC share common combustion sources, allowing the POC/EC ratio to serve as an indicator to identify the primary sources, which can be determined by utilizing the minimum ratio (MIN) method (Castro et al., 1999). This assumption is less justified and

65   compromised with naiveté, as observed OC/EC ratios can span over one order of magnitude in ambient measurements, which could be affected by measurement artifacts and fluctuate under different meteorological conditions (Yuan et al., 2006). Furthermore, the lack of a widely accepted criterion for percentile selection can bring up the bias to SOC estimation (Wu et al., 2019). The minimum R squared (MRS) method is a less arbitrary approach to determine the POC/EC ratio for primary sources. In MRS, the optimal primary POC/EC ratio is determined by minimizing the

70   Pearson's correlation coefficient between EC and deduced SOC (Wu and Yu, 2016). The MRS method has been

increasingly used in studies with the hourly measurements in various environments (Bian et al., 2018; Wu et al., 2019; Yao et al., 2020). However, it has been proven that the MRS method inevitably yields a POC/EC ratio that renders EC and deduced SOC completely uncorrelated. This contradicts our expectation of a weak yet not negligible correlation between EC and SOC, since some SOC species could be formed from precursors co-emitted with EC through

75   combustion activities (Deng et al., 2020; Gentner et al., 2017; Jathar et al., 2013), and both SOC and EC are influenced by regional transport or changes in the boundary layer height. On the other hand, the MLR model is a powerful statistical tool to estimate SOC by considering highly associated variables rather than the difference between measured OC and estimated POC (Kim et al., 2012; Pachon et al., 2010). Another approach, the secondary organic aerosol (SOA) tracer method, utilizes SOA tracer yield data derived from chamber experiments to estimate the SOC and SOA

80   contributions from several precursors (Kleindienst et al., 2012; Kleindienst et al., 2007). However, the availability of SOA tracer data are limited to only a small number of  common precursors, leading to a bias in the quantification of SOC mass (Cheng et al., 2021).

Compared to the above-mentioned approaches, our research group has recently developed a novel Bayesian inference (BI) method that allows for the quantification of POC and SOC based on measurement data of PM major components

85   (i.e., OC, EC, and major secondary inorganic ions). This approach provides better agreement with tracer-based PMF results than traditional techniques. The principle of this approach can be found in Liao et al. (2023). Briefly, our method differentiates POC and SOC by incorporating prior knowledge and measurement data of major PM components to make probabilistic inferences about the unknown POC and SOC mass. This is achieved by considering the parameters as random variables rather than constants, which distinguishes it from the multiple linear regression

90   model. This innovation in methodology offers the potential for quantifying POC and SOC with higher accuracy and lower computational complexity.

Hong Kong is located in southern China and is part of the Guangdong–Hong Kong–Macau Greater Bay Area (GBA) economic and business hub. Since the implementation of the Clean Air Plan in 2013 by the Hong Kong Environment Bureau, air pollution in Hong Kong has significantly improved (Hong Kong Environment Bureau, Bureau, 2013).

95   Numerous studies have been conducted to measure variations in chemical speciation components and potential sources over the past years, but are mainly based on 24-hour offline filter measurements (Cao et al., 2003; Hu et al., 2010; Li et al., 2013). As such, information on POC and SOC in $PM_{2.5}$ are unavailable in time scales down to hourly and for continuous and extended duration covering all seasons.  The limited temporal resolution of previous studies has prevented the exploration of diurnal variations and rapid evolutionary processes, which are crucial for understanding

100   SOC formation in the ambient environment. Moreover, long-term continuous measurements are limited in Hong Kong, hindering our comprehensive understanding of episodic events occurring under different seasonal synoptic conditions.

In this study, continuous online monitoring of atmospheric $PM_{2.5}$ and carbonaceous components (i.e., OC and EC) was carried out at a regional suburban site in Hong Kong for nearly one year and a half from 16 July 2020 to 31 December 2021. The objectives of this study are threefold: (1) to identify the optimal method setup and to derive hourly POC

105   and SOC using the novel Bayesian inference approach; (2) to characterize variations of POC and SOC at multi-temporal scales, including diurnal, weekday/weekend, and seasonal variations, and to identify factors influencing SOC

formation; and (3) to investigate SOC variations during city-wide high-PM$_{2.5}$ episodes under different seasonal synoptic conditions. The methodology of this work could serve as a valuable guide for other locations with similar monitoring capabilities. The observation-based POC and SOC data and insights gained regarding pollution processes
110   will provide valuable observation constraints for improving air quality models for our region and other locations.

## 2 Methodology

### 2.1 Aerosol sampling and measurement

The aerosol measurements were conducted at the Hong Kong University of Science and Technology Air Quality Research Supersite (HKUST supersite), which is located on the HKUST campus. Detailed description of this site can
115   be referred to our previous papers (Li et al., 2022; Wang et al., 2022b). Briefly, The HKUST supersite is situated on the hillside of Clear Water Bay in the eastern coastal area of Hong Kong (22.33°N, 114.27°E). The site is characterized by the prevalence of evergreen broadleaved woods as the dominant vegetation type. It is a low-moderately polluted site with limited local anthropogenic emissions from a dormitory construction site and a small canteen in the vicinity. The construction site operates from 09:00-18:00 (local time) from Monday to Saturday. The operation of the canteen
120   has been scaled down to minimum levels due to the ongoing pandemic during the study period.

The sampling period lasted for nearly a year and a half from 16 July 2020 to 31 December 2021. Multiple online instruments of hourly or higher time-resolution were deployed to measure the PM$_{2.5}$ levels, its major components as well as gaseous pollutants and meteorological parameters. Briefly, PM$_{2.5}$ mass concentrations were measured by a SHARP monitor (Model 5030i; Thermo Fisher Scientific, USA); major water-soluble inorganic ions (sulfate, nitrate,
125   and ammonium) were monitored by a monitor for aerosols and gases in ambient air (MARGA 1S; Metrohm AG, Switzerland); carbonaceous components (organic carbon, OC, and elemental carbon, EC) were determined by a semicontinuous OC/EC analyzer (model RT-3179; Sunset Laboratory Inc., Oregan, USA). Gaseous pollutants (O$_3$, NO, and NO$_x$) were measured by gas analyzers (Teledyne API 400A, USA; Ecotech Serinus 40, USA, respectively). Meteorological parameters, including temperature, relative humidity (RH), wind speed (WS) and wind direction (WD)
130   were measured by the 10 m automatic weather station (AWS tower, Model 6000, Belfort Instrument Company, USA). The output data from all the above-mentioned instruments were averaged at a resolution of 1-h, and appropriately aligned for the subsequent analysis. The PM$_{2.5}$ levels and gas pollutant data in a nearby rural station (Tap Mun) ~15 km to the northeast were used as reference for days before Oct 2020 and after Nov 2021, during which the respective instruments at our sites were either unavailable or under maintenance. The details in treatment for the missing data
135   can be found in our previous studies (Wang et al., 2022b).

### 2.2 Estimation of secondary and primary organic carbon by the Bayesian Inference approach

In this study, the estimation of POC and SOC were performed by the Bayesian Inference approach, which is newly developed in our group (Liao et al., 2023). This method relies on only major chemical composition data that are commonly measured. Specifically, the concentrations of primary and secondary OC are calculated based on Eq. 1-2:

$$OC = EC \times K_1 + SIA \times K_2 \tag{1}$$

$$POC = EC \times K_1, and\ SOC = SIA \times K_2 \tag{2}$$

where OC and EC are the measured hourly concentrations of OC and EC; SIA represents one of the major secondary inorganic ions (i.e., $SO_4^{2-}$, $NO_3^-$, and $NH_4^+$); $K_1$ and $K_2$ are POC/EC ratio and SOC/SIA ratio that are yet to be deduced using Eq. (3).

$$\pi(K_1, K_2|Data) = \frac{L(Data|K_1, K_2)p(K_1, K_2)}{\int L(Data|K_1, K_2)p(K_1, K_2)dK_1 dK_2} \tag{3}$$

where $p(K_1, K_2)$ is the prior distribution of $(K_1, K_2)$, $L(Data|K_1, K_2)$ is the likelihood function of observation data , and $\pi(K_1, K_2|Data)$ is the posterior distribution to be determined. The BI principle is rooted in Bayesian's theorem and embodied in Eq. 3. With the aim of determining the posterior distribution, we first find out the likelihood function $L(Data|K_1, K_2)$ of observation data with respect to parameters to estimate and the prior distribution of such parameter. Eq (4) gives the likelihood function in our Bayesian model by assuming a normal distributed error term.

$$OC \sim N(EC \times K_1 + SIA \times K_2, \sigma_{EC}^2 \times K_1^2 + \sigma_{SIA}^2 \times K_2^2 + \sigma_{OC}^2) \tag{4}$$

Where $\sigma_{EC}$, $\sigma_{OC}$, and $\sigma_{SIA}$ are the uncertainties for EC, OC, and SIA, respectively. The prior distributions of $K_1$ and $K_2$ are set following Eq. 5, signifying the prior knowledge of these two ratios before analyzing the observation data.

$$K_1 \sim N(2.0, 1.0^2), and\ K_2 \sim N(0.4, 0.2^2) \tag{5}$$

Liao et al. (2023) recommend setting these two prior distributions fairly wide to avoid unnecessary constraints, and according to their sensitivity analysis, the influence from different prior distributions becomes negligible when there are adequate observation data. Based on our experience of applying Bayesian inference to estimate POC and SOC, when there are around 10 or more observations in one dataset, estimated posterior distribution of $(K_1, K_2)$ will be robust enough regardless of the prior distribution. Given that the posterior distribution of $(K_1, K_2)$ cannot be solved analytically, we resort to Markov Chain Monte Carlo (MCMC) sampling for numerical estimation, where we construct a Markov chain whose limit distribution is the same as the posterior distribution of interest. The mean values of $(K_1, K_2)$ from such sampling are then used to deduce POC and SOC using Eq. 2.

Finally, from basic error propagation analysis, we further define the uncertainties of POC and SOC (i.e., $\sigma_{POC}$ and $\sigma_{SOC}$) as per Eq. 6:

$$\sigma_{POC} = POC \times \sqrt{(\frac{\sigma_{EC}}{EC})^2 + (\frac{\sigma_{K_1}}{K_1})^2}, and\ \sigma_{SOC} = SOC \times \sqrt{(\frac{\sigma_{SIA}}{SIA})^2 + (\frac{\sigma_{K_2}}{K_2})^2} \tag{6}$$

Compared to other statistical methods (i.e., MIN, MRS, and MLR methods), the BI method allows greater flexibility in model establishment and comprehensive consideration of all measurement uncertainties.

**2.3 Auxiliary analysis**

The aerosol water content (AWC), and acidity were calculated by the thermodynamic equilibrium model ISORROPIA

170     II (http://nenes.eas.gatech.edu/ISORROPIA). The calculation is performed based on the assumption that the aerosol is in metastable state and at chemical equilibrium between the aerosol and gas phase. The model is set in forward mode, with the inputs of aerosol phase $Na^+$, $K^+$, $Mg^{2+}$, $Ca^{2+}$, $NH_4^+$, $NO_3^-$, $SO_4^{2-}$, gas phase $HCl$, $HNO_3$, $NH_3$, ambient temperature, and RH.

### 3 Results and discussion

175     **3.1 Determination of POC and SOC by the BI method**

Considering the emission sources and secondary formation processes would vary from season to season, we quantified POC and SOC in each individual season to account for seasonal variations. The division of seasons was based on upper-level wind direction, sea-level pressure, and dew point (Wong et al., 2022; Yu, 2002), as shown in Figure S1. Specifically, the seasons were 2020 summer (16 July-28 September 2020), 2020 fall (8 October-23 November 2020),

180     2020-2021 winter (24 November 2020-28 February 2021), 2021 spring (1 March-2 May 2021), 2021 summer (3 May-7 October 2021), 2021 fall (8 October-24 November 2021) and 2021 winter (25 November-31 December 2021). Within each season, the data was further divided into $24 \times 4$ groups based on same individual hours and wind direction. The BI model was then applied to each group of data. The BI method's inherent advantage allows for this fine division of measurement data, which ensures relatively constant $K_1$ and $K_2$ within each group.

185     Regarding the selection of the optimal SIA species for tracking SOA in the BI method, Liao et al. (2023) found that the simulation results using sulfate or ammonium as the SOC tracer yielded better agreement with the reference results compared using nitrate. This discrepancy could be attributed to larger measurement artifacts associated with evaporation loss of nitrate in the offline measured data set. For the online measurements, the simulation results using nitrate were also inferior to those using sulfate or ammonium, as the formed SOA is largely retained in the fine particles,

190     while nitrate has propensity to partition onto coarse particles. To further determine the optimal SOC tracers, an uncertainty analysis utilizing an error estimation method was conducted. As shown in Figure S3a, the absolute concentration and uncertainty of POC were highly correlated and showed minimal difference between BI-$SO_4^{2-}$ and BI-$NH_4^+$, whereas the uncertainties for SOC were much larger by BI-$SO_4^{2-}$ than BI-$NH_4^+$. The relative uncertainty, calculated as the uncertainty divided by the concentration, yielded comparable values for POC with both indicators

195     (Figure S3b), while BI-$NH_4^+$ generated larger relative uncertainties for SOC compared to BI-$SO_4^{2-}$. This suggests that sulfate is a better tracer for quantifying SOC levels in our dataset. This conclusion is further supported by a statistical criterion, the Bayesian Information Criterion (BIC), which is universally used in model selection. Lower BIC values indicate better modelling results. The BIC values for the three SOC tracers were calculated for each individual season, with sulfate consistently yielding the lowest value (Table S1). Thus, the BI-derived POC and SOC using sulfate as the

200     SOC tracer are considered to provide more accurate data with lower uncertainties and are consequently adopted in the subsequent analysis.

Figure 1 shows the distribution and seasonal variations of $K_1$ and $K_2$ values determined for the $24 \times 4$ groups. The POC/EC ratio ($K_1$) is influenced by the predominant primary sources and meteorological conditions. Due to the

monsoon shift in Hong Kong, air pollution during summer is primarily under the control of local emissions, while in
205    cold seasons, regional transport from the continent to the north has a dominant influence. Hence, different predominant
sources for POC and EC in Hong Kong are expected. Additionally, many POC species in $PM_{2.5}$ are semi-volatile and
are subject to gas-phase partitioning equilibrium, leading to more POC retained in the particle phase at lower
temperatures. These factors contribute to a higher $K_1$ values in winter compared to summer (Figure 1a) ($p < 0.01$), and
a more pronounced diurnal pattern in summer (Figure 1b). On the other hand, SOC/SIA ratio ($K_2$) is influenced by the
210    sources of their precursors, the strength of secondary formation in the atmosphere, and meteorological parameters.
Figure 1a shows that $K_2$ is higher (larger mean values) and less variable (smaller inter-quantile ranges) in winter ($p <$
0.01), and Figure 1b demonstrates that hourly $K_2$ values are more stable in winter compared to summer. The long-
range regional transport during winter could account for the reduced variability in $K_2$ during cold seasons.
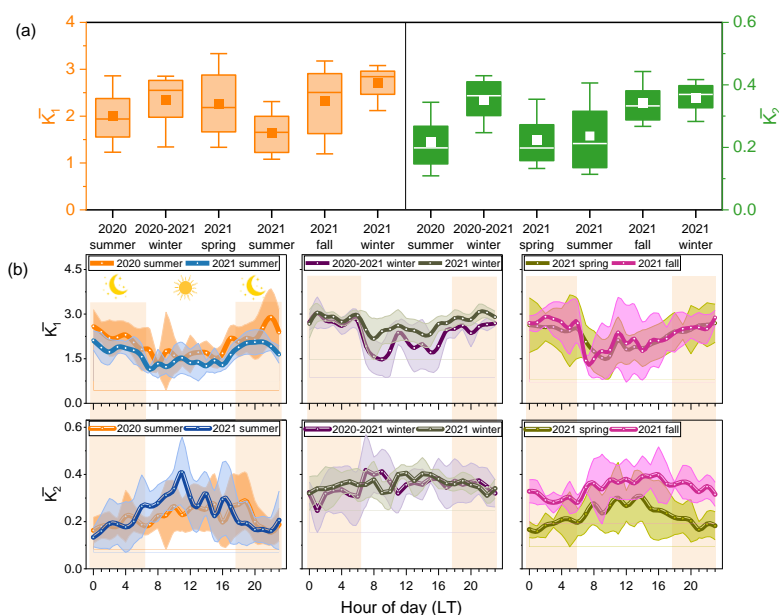
215    **Figure 1. (a) Box plot of $\overline{K_1}$ and $\overline{K_2}$ values across different seasons (the lower and upper boundaries of the boxes represent
the 25% and 75% percentile values, and the squares and horizontal lines in the box denote the average and median,
respectively). (b) The diurnal variations of $\overline{K_1}$ and $\overline{K_2}$ in individual seasons (solid lines represent the average values, area
indicate standard deviation).**

During the periods of 2020-2021 winter and 2021 spring, we have conducted source apportionment analysis using
220    PMF based on a suite of elemental and molecular tracer data in $PM_{2.5}$. The PMF results provide an independent means
to determine POC and SOC. Detailed discussions on the SOC and POC from PMF are documented in our previous
publication (Wang et al., 2023a; Wang et al., 2023b). Figure S2 compares POC and SOC estimates obtained from the
BI approach versus the PMF method. Good agreements were found between the two methods for POC in both seasons
($r > 0.8$). However, the correlations for SOC exhibited slightly lower correlation coefficient in spring. The discrepancy
225    in spring could be due to the majority of PMF-resolved SOC associated with the biogenic secondary organic aerosols
factor rather than the secondary sulfate factor (Wang et al., 2023b). Nevertheless, the overall strong agreement between

the BI approach and PMF indicates that the BI approach can accurately estimate POC and SOC levels and is applicable across different seasons.

## 3.2 Multi-temporal scale variations of POC and SOC

### 3.2.1 Annual levels and seasonal variations

Figure 2a shows the time series of meteorological parameters, gaseous pollutants, $PM_{2.5}$ and the carbonaceous components, including OC, EC, POC and SOC over the entire measurement period. The study-wide $PM_{2.5}$ concentrations ranged from 1.0 to 94 μg m$^{-3}$ with an average of 14.8 ± 8.8 μg m$^{-3}$. The $PM_{2.5}$ levels varied notably from hour to hour, with 14% exceeding 25 μg m$^{-3}$. This value (25 μg m$^{-3}$) is the new $PM_{2.5}$ annual Interim Target-2 "Air Quality Guidelines (AQG)" recommended by the World Health Organization. It is also the newly proposed Air Quality Objective for $PM_{2.5}$ by the Hong Kong Government (Hong Kong Environment Bureau, Bureau, 2021). The $O_3$ and $NO_x$ concentrations throughout the studied period had an average value of 44 ± 19 ppb and 8.9 ± 7.8 ppb, respectively. The concentrations of OC varied from 0.06-15.7 μgC m$^{-3}$ (avg. 2.8 ± 2.0 μgC m$^{-3}$), and EC ranged from 0.02-6.4 μgC m$^{-3}$ (avg. 0.76 ± 0.64 μgC m$^{-3}$). POC was 1.6 ± 1.3 μgC m$^{-3}$ on average (range: 0.06 to 12.4 μgC m$^{-3}$), approximately two times the average SOC concentration (avg. 0.92 ± 0.74 μgC m$^{-3}$, range: 0.02 to 6.8 μgC m$^{-3}$). The SOC percentage contributions varied under different environments due to the complex sources and formation processes, as well as the meteorological conditions. The contribution of SOC in percentage at our sampling site was lower than those measurements in urban Hong Kong, and other urban cities (Li et al., 2020; Zhou et al., 2014; Zhu et al., 2021), but comparable to a similar suburban site in Shanghai (Wang et al., 2022a; Wang et al., 2022c).

As a sub-tropical region in the southeast coastal of China, the sampling site is under the influence of the seasonal evolution of the East Asian Monsoon system, exhibiting distinctive season-dependent air pollution characteristics. During the summertime, the prevailing wind is from southern oceanic areas, while north-westerlies wind dominated in the winter. Spring and autumn are transitional seasons in between. The RH levels were > 80% in spring and summer, considerably higher than in fall (~70%) and winter (~60%). The wind speeds during winter and fall were higher compared to summer and spring, with the prevailing airflow coming from northwest (Figure 2b). These meteorological conditions would favor the transport and dispersion of air pollutants over larger scale in winter over summer. The seasonal variations in $PM_{2.5}$ showed higher levels in winter and fall compared to spring and summer. $NO_x$ showed the highest levels in the summer and fall of 2021 due to the accumulation of local vehicle emissions from the nearby construction activities, while $O_3$ showed distinct variations with the generally lowest levels in summer. The summer low ozone is attributed to the prevailing southerly flow introduced by the summer monsoon which brings less $O_3$ and /or $O_3$ precursor (So and Wang, 2003). Besides, the strong ozone titration effects by higher $NO_x$ levels could be also responsible for the decreased $O_3$ levels in summer (Zhang et al., 2013). The seasonal variation trends of OC and EC were consistent, with higher concentrations in winter, followed by fall, spring and summer. Similarly, POC and SOC levels were highest in winter and lowest in summer, showing a difference of ~3 times (2.9 vs. 0.8 μgC m$^{-3}$ and 1.5 vs. 0.5 μgC m$^{-3}$, respectively) between the two seasons. With regards to the interannual variations, the levels $PM_{2.5}$ and its carbonaceous components exhibited relatively less variations, with comparable levels observed in the same season

across different years.
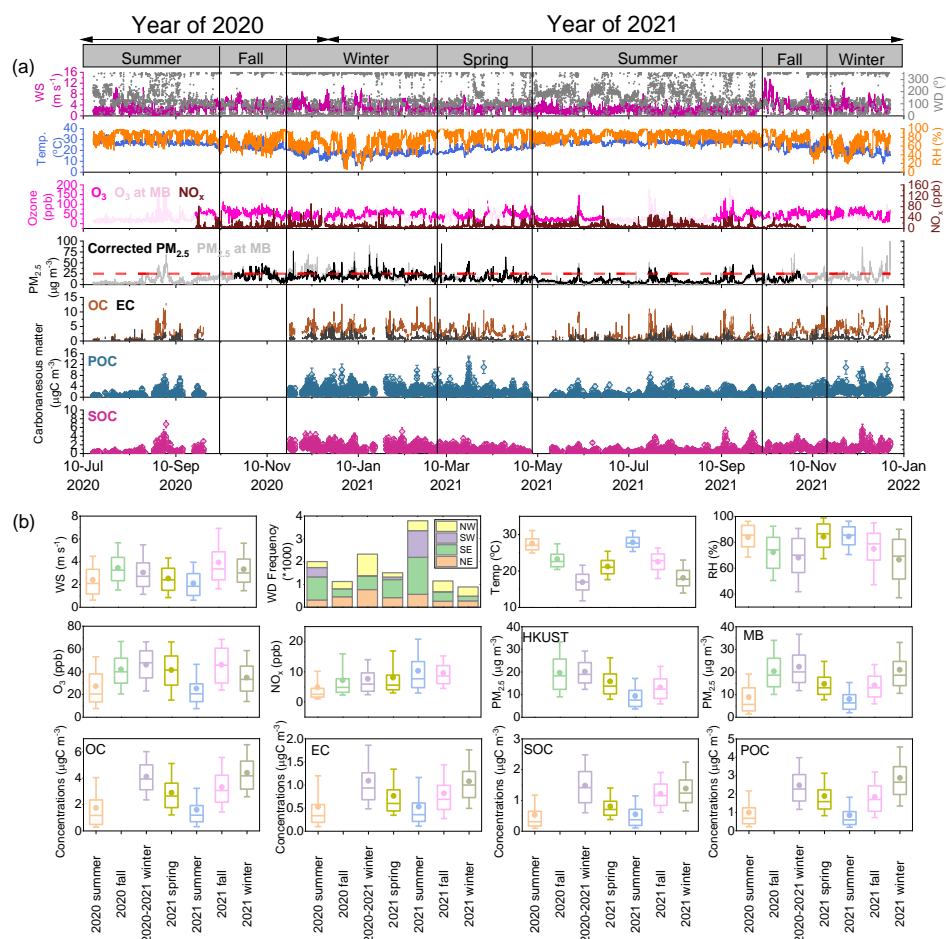
**Figure 2. (a) Time series and (b) Seasonal variations of meteorological parameters (wind speed, wind direction, temperature, and RH), gaseous pollutants (O₃, and NOₓ), PM₂.₅ (the red dash line marks the WHO AQG IT-4 value), OC and EC, as well as POC and SOC during the observation period (16 July 2020–31 December 2021) at the HKUST supersite.**

### 3.2.2 Weekend-weekday pattern and diurnal variations

The diurnal variations of $PM_{2.5}$, $O_3$, $NO_x$, and carbonaceous components over the entire period are shown in Figure 3. Since the sampling location is situated near a construction site, we conducted a comparative analysis of diurnal variations between weekdays and weekends to evaluate the influence of construction activities on aerosol particles and gas pollutants. $PM_{2.5}$ displayed minimal disparities between weekdays and weekends, showing flat diurnal cycles across various seasons, except for the winter of 2021. During this particular winter, higher concentrations of $PM_{2.5}$ were observed at night on weekends compared to weekdays. The diurnal variations in $O_3$ exhibited clear daily trends throughout different seasons, with higher concentrations during daytime and a peak in the late afternoon. These

275   patterns closely correspond to variations in radiation and temperature. The daily variations of $NO_x$ showed a clear diurnal pattern with higher daytime concentrations on weekdays, which is characterized by two concentration peaks at 9-10 am and 16-18 pm, aligning with the traffic peak hours at the start and at the end of a working day at the construction site. Similarly, EC showed pronounced two peaks during the daytime on weekdays across different seasons, further indicating the noticeable impacts of primary traffic emissions on $NO_x$ and EC levels, particularly on

280   workdays. Conversely, $NO_x$ and EC levels were generally lower on weekends and lacked a distinct diurnal variation. Different from EC, OC showed less difference between weekdays and Sundays. Slightly higher daytime concentrations with a peak around noon were observed in the two summer seasons, which could be attributed to the enhanced photochemical formation of OC. Diurnal cycles of OC were flatter in other seasons. The higher OC/EC ratios (Figure S4d) were observed during weekends across different seasons, providing additional evidence of reduced

285   vehicle emissions on non-working days.
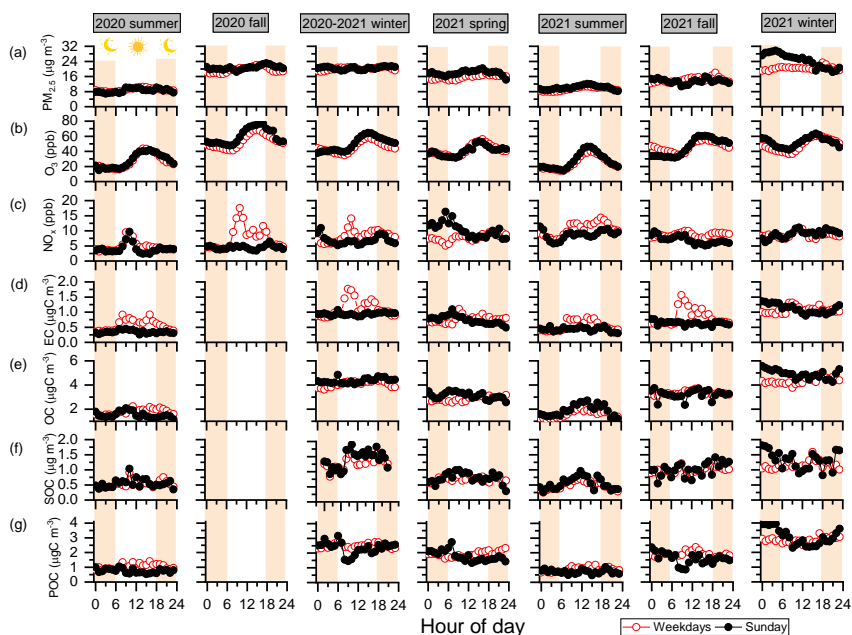
**Figure 3. Diurnal variations of (a) PM$_{2.5}$, (b) O$_3$, (c) NO$_x$, (d) OC, (e) EC, (f) POC and (g) SOC over the entire measurement period. The circles represent the hourly data averaged over weekdays (Monday -Saturday, red) and Sunday (black). The light orange shades represent nighttime periods.**

290   The weekday-weekend patterns of POC and SOC displayed notable distinctions. Specifically, SOC levels remained comparable between working days and weekends, whereas POC was slightly higher on weekdays throughout different seasons. This observation suggests that nearby construction site emissions exerted a stronger influence on POC levels, while SOC formation appeared to be more influenced by biogenic precursor emissions at our site. Regarding diurnal variations, POC exhibited comparable levels during nighttime on both weekdays and weekends, while higher levels

295   were observed during daytime on working days. The much higher POC/SOC ratios during daytime on weekdays

(Figure S4e) further collaborated on the impact of primary emissions on POC. Additionally, the SOC levels showed increased concentrations during daytime on both weekdays and weekends, similar to the daily patterns of $O_3$ as shown in Figure S4b, indicating the influence of photochemical reactions. It should be noted that SOC formation processes are complex and influenced by various factors, including ambient atmospheric oxidants and precursors levels.

300 Moreover, these reactions are significantly influenced by meteorological parameters. Further investigation into the relationships between SOC formation and the aforementioned factors (i.e., temperature, RH, $O_3$ and $NO_x$) will be described in **Sec.3.3.**

### 3.3 Characterization of SOC formation dependence on meteorological conditions, $O_x$ and $NO_x$ levels

The dataset was divided into five groups based on $PM_{2.5}$ concentrations in individual seasons to investigate the SOC

305 formation under varying pollution conditions. Specifically, periods of $PM_{2.5} < 5$ μg m$^{-3}$ represents the extremely clean condition; interval of 5 μg m$^{-3}$ < $PM_{2.5}$ < 10 μg m$^{-3}$ represents the clean condition; interval of 10 μg m$^{-3}$ < $PM_{2.5}$ < 15 μg m$^{-3}$, represents the low-pollution condition; interval of 15 μg m$^{-3}$ < $PM_{2.5}$ < 25 μg m$^{-3}$, represents the medium-pollution condition; and interval of 25 μg m$^{-3}$ < $PM_{2.5}$, represents the high-pollution condition. The definition of $PM_{2.5}$ transition value aligns with the annual AQG level, and the Interim Target 2 to 4 limits set by WHO. The evolution of

310 SOC with the increase in the meteorological parameters (i.e., temperature and RH) during different seasons within the same pollution conditions are shown in Figure 4. SOC concentrations were generally low in low-PM conditions but increased significantly with the intensification of pollution. The highest SOC levels were observed in periods with $PM_{2.5} > 25$ μg m$^{-3}$ during all the seasons, indicating intensive SOC formation contributing to $PM_{2.5}$ air pollution.
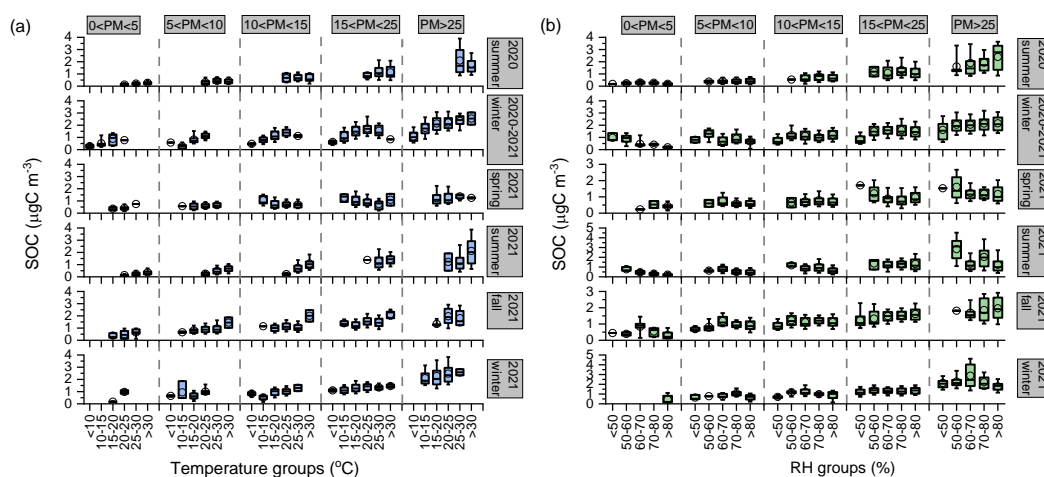
315 **Figure 4. Concentrations of SOC as a function of (a) temperature bins and (b) RH bins under different $PM_{2.5}$ groups in individual seasons during the entire measurement period. The markers represent the mean values, and whiskers represent the 25$^{th}$ and 75$^{th}$ percentiles.**

As shown in Figure 4a, the average concentrations of SOC were lower than 1 μgC m$^{-3}$ when T < 15°C in all seasons under different pollution conditions, and increased notably with the increasing temperature, reaching the highest levels

320   at T > 30°C. The peak concentrations were almost twice of those in T <10°C. These results highlight the important role of temperature in boosting the ambient SOC formation. Previous chamber experiments and field observations have found that increasing temperature could not only promote the emissions of biogenic VOCs emissions, but also enhance the oxidation reactions (Ding et al., 2011; Svendby et al., 2008). The positive trends were much clear especially in fall and winter during the pollution conditions (PM > 10 μg m$^{-3}$), suggesting that the effects of

325   temperature would be more remarkable on SOC formation in cold seasons. This is further confirmed by the stronger Pearson correlation coefficients ($R_p$) in winter and fall ($r$=0.42-0.57) than in spring and summer ($r$ = 0.10-0.35).

In contrast to temperature dependence, SOC was less sensitive to RH in all seasons and did not exhibit clear trend (Figure 4b). Under the clean and low PM pollution conditions, SOC showed a much flatter trend with the increasing in RH. At the medium PM pollution conditions, highest SOC levels were observed in low RH groups (RH<60%) and

330   did not change extensively in high RH groups, while under high PM pollution condition, the responses of SOC to RH groups varied across different seasons. In the summer period, SOC levels showed less variations in 2020, while in 2021, highest SOC concentrations occurred in the low RH groups (50%<RH<60%), and then decreased with the increased in RH. The SOC behaviors in the two winter periods were also different, with comparable concentrations across the RH groups in 2020, but much higher SOC levels in the medium RH group in 2021. The SOC behaviors in

335   spring and fall seasons exhibited less variations with the RH groups. The weak relationship between SOC and RH suggested that aqueous phase chemistry may not be the major formation pathway of SOC in our site, which is different from observations in northern China (Guo et al., 2012; Wang et al., 2012) but similar to the location with comparable site characteristics in suburban Shanghai (Wang et al., 2022a).

The relationships between SOC and atmospheric oxidants $O_x$ levels under different pollution conditions in individual

340   seasons are shown in Figure 5a. Atmospheric oxidants $O_x$ ($O_3$+$NO_2$) can be utilized to indicate the ability of atmospheric oxidation associated with photochemical reactions (Kley et al., 1994; Notario et al., 2013). A previous offline measurement study in Hong Kong reported positive correlations between SOC and $O_3$ and highlighted that SOC formation was sensitive to the oxidant levels (Hu et al., 2008). In this study, SOC levels in spring and summer were less sensitive to the $O_x$ under low and medium PM pollution conditions (PM < 25 ug m$^{-3}$). But under the high

345   PM pollution condition, the enhancement of SOC with increase in $O_x$ was only found when $O_x$ < 100 ppb; as $O_x$ further increased, SOC started to decline. In winter, SOC levels showed a clear positive trend with increasing $O_x$, especially under medium and high PM pollution conditions. The daily highest $O_x$ is commonly seen at noontime to late afternoon when the solar radiation is the strongest. The strong positive correlations of SOC with $O_x$ in winter highlighted that the photochemical formation might remain highly efficient and play an important role in contributing to high SOC

350   levels and air pollution.

The associations of SOC with the $NO_x$ are shown in Figure 5b. Under the clean and medium pollution conditions, the trends between SOC and $NO_x$ were less clear across all the seasons. However, the variations under pollution conditions differed in individual seasons. The concentrations of SOC increased substantially with $NO_x$ in two summer periods under the pollution conditions, suggesting that $NO_x$ can also be essential to the SOC formation in contributing to

355   photochemical air pollution in summer period (Fan et al., 2022; Roberts, 1990). However, during the winter seasons,

when the air masses were dominated by the long-ranged air masses originated from northern China, SOC levels were slightly higher in low $NO_x$ groups than those in high $NO_x$ groups. It's noted that the variations of SOC with $NO_x$ were distinct from those of SOC with $O_3$ in summer and winter seasons, especially under high pollution conditions. These results suggest that the SOC formation pathways are different and might be promoted by various oxidants under different ambient environments.
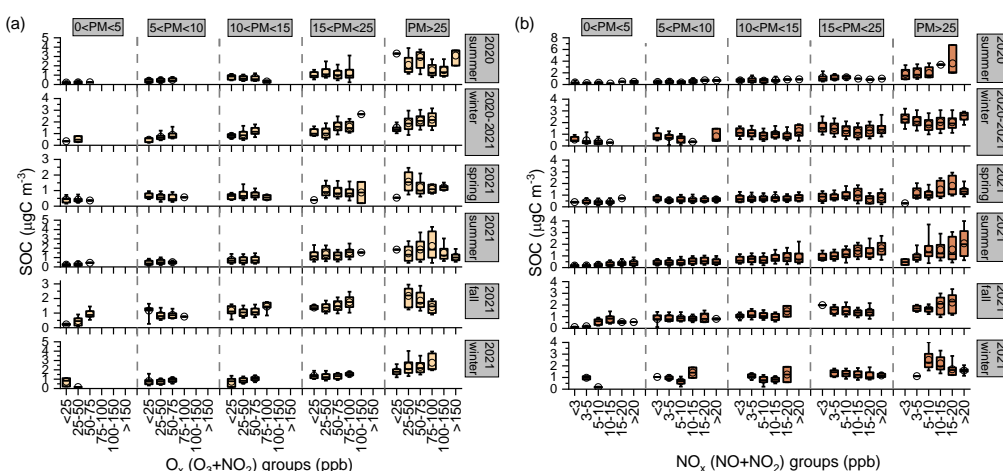
**Figure 5. Concentrations of SOC as a function of (a) $O_x$ bins (b) $NO_x$ bins under different $PM_{2.5}$ groups in individual seasons during the entire measurement period. The markers represent the mean values, and whiskers represent the 25th and 75th percentiles.**

### 3.4 Evolution characteristics of SOC during the city-wide $PM_{2.5}$ episodes

#### 3.4.1 Classification of city-wide $PM_{2.5}$ episodes

As mentioned above, high SOC levels were observed under pollution conditions with $PM_{2.5}$ higher than 25 µg m⁻³. We further extract the pollution hours to examine the SOC features for gaining insights into its formation mechanisms. We have identified a total of 65 pollution episodes based on a screening method using city-wide air pollutant data from 15 general monitoring stations operated by Hong Kong Environment Protection Department (HKEPD) rather than a single site. The site characteristics and geographical locations of the monitoring stations are shown in Figure S5. The details of this method can be found in our previous publication (Wang et al., 2022b). In the ensuring analysis, $PM_{2.5}$ episodes were identified as periods of hourly concentrations exceeding 25 µg m⁻³ and lasting 6 consecutive hours or longer at more than three monitoring stations. Figure S6 shows the average concentrations of $PM_{2.5}$ across the 15 stations during individual episodes and those during the non-episode hours. The statistical summary of episode information, $PM_{2.5}$ averages, the meteorological conditions, and the gas pollutants ($O_3$ and $NO_x$) during individual episodes are listed in Table S2.

As expected, pollution episodes occurred more often in winter (i.e., 24 in 2020-2021 winter, and 7 in 2021 winter, respectively) than in summer and fall. This can be attributed to the less wet deposition and elevated contributions from

380   regional transport, which could be further confirmed by the higher wind speed. We also observed 14 episodes in 2021 spring, possibly due to the dust storms from outside Hong Kong (Ding et al., 2005; Wang et al., 2004). The city-wide PM$_{2.5}$ max-to-min ratios of individual episodes are calculated to investigate the spatial variations (Table S2). A ratio close to 1 indicates the episodic pollution was spatially homogeneous in Hong Kong; a higher value means higher spatial heterogeneity of the episodes across Hong Kong. Generally, the ratios in summer and fall episodes were lower

385   than 2, while higher ratios were observed in winter and spring episodes, indicating the spatial gradient was more notable under the regional influences.

### 3.4.2 Variations in SOC during the episodes

The average concentrations of gaseous pollutants, PM$_{2.5}$, POC and SOC are shown in Figure 6a-e. In general, the concentrations in non-episode hours were higher in winter and fall than those in spring and summer, suggesting the

390   consistent influences of regional transport. Higher concentrations of O$_3$ were observed in winter and fall episodes, with episodes-average of 29-78 ppb, except EP11, EP20 and EP52. It's noted that NO$_x$ levels in these three episodes were much higher than the others. Summer episodes had significantly higher levels, with average concentrations that were more than 2 times than the other seasons. The mass increment ratio (MIR) is calculated as the mass concentration during the episode divided by that during the non-episode hours in the same season, which could be used as an

395   indicator to evaluate the change in the concentration during the episode. The MIR values of O$_3$ and NO$_x$ were generally larger than 1 during the summer and spring episodes (Figure 6g), while close to 1 during winter. In contrast to the gaseous pollutants, the average concentrations of episodic PM$_{2.5}$ showed less seasonal variations, with slightly lower values in 2021 fall. The MIR values were larger than 1 during the majority of episodes, with the highest values in summer (~2-5) and fall (~1.5-2.2) episodes.

400   The concentrations of carbonaceous components were much higher during episodes than non-episode hours in the same seasons. POC levels were higher in winter episodes, while SOC showed enhancement across different seasons except spring (Figure 6d-e). MIR values >1 were observed for both POC and SOC during summer episodes, with noticeably larger MIR values exceeding 2. Lower MIR values were found in winter seasons, possibly due to the high background levels. The percentage contributions of POC and SOC during individual episodes are shown in Figure 6f.

405   The SOC mass fraction varied in individual seasons, ranging from 10% in EP43 to 66% in EP09. Compared with the corresponding values in non-episode hours, higher SOC percentages were generally found in winter and summer episodes, while they were similar in fall and spring episodes. It is worth noting that the meteorological conditions and major atmospheric oxidants are different in the two seasons, indicating that the formation mechanism differs in the two seasons. Further examination of SOC variations during summer and winter episodes would enhance understanding

410   of SOC formation mechanisms, which will be described in the subsequent sections.
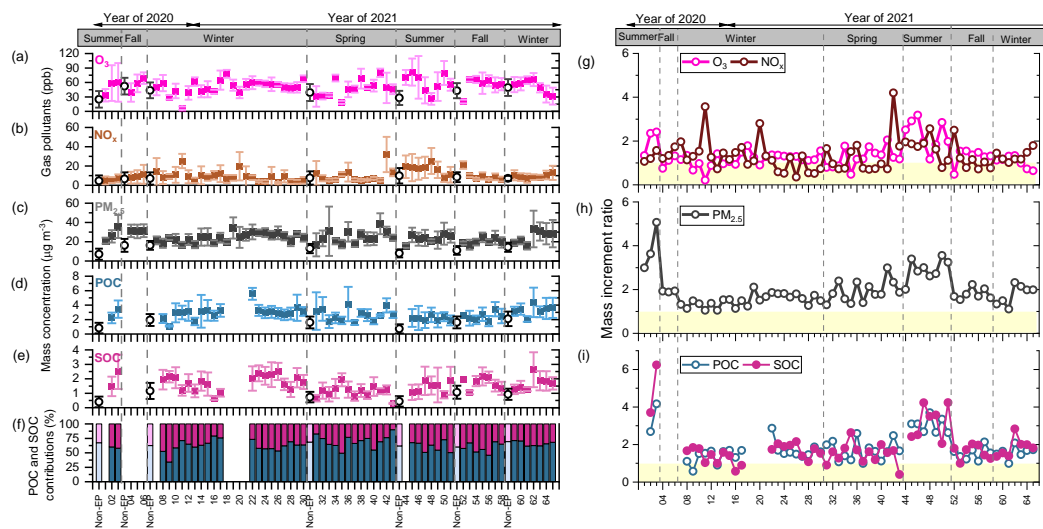
**Figure 6. Comparison of select pollutant levels during episodes and non-episodes for individual episodes. The comparison parameters include concentrations of (a) O₃, (b) NOₓ, (c) PM₂.₅, (d) POC, and (e) SOC, (f) POC and SOC percentage contributions, and mass increment ratios of (g) O₃ and NOₓ, (h) PM₂.₅, and (i) POC and SOC. In panels (a)-(e), the filled squares represent during-episode concentrations while the empty circles represent non-episode concentrations. In panels (g)-(i), the light-yellow shaded zone marks values mass increment ratios of less than 1.**

### 3.4.3 Summer typhoon-related episodes

Out of a total of 8 episodes in summer 2021, 7 of them were mainly caused by the tropical typhoons. Names and tracks of these typhoons are shown in Figure S7. During the episodes, winds come from multiple directions with relatively low wind speed ($<2$ m s$^{-1}$), so that the stagnant conditions could favor the accumulation of air pollutants. Episodic PM₂.₅ concentrations did not show clear spatial gradient, suggesting that the air pollution was possibly attributed to local emissions.

As shown in Figure 7a, concurrent enhancements of gas pollutants and PM₂.₅ mass loadings were observed during the episodes. PM₂.₅ concentrations notably increased with typhoon evolution, reaching peak values of nearly 50 μg m$^{-3}$ except for EP48. The highest O₃ levels were observed at noon under the influence of Chaiwan and Chanthu2 (EP45 and EP50, respectively). Extremely low NOₓ levels were observed in EP50 with an average of 7.7 ppb. POC and SOC levels largely increased during the episodes, with different responses in individual episodes. Specifically, a sharp increase in POC was observed in EP45, but SOC levels did not increase noticeably. Similar results were observed in EP46, EP48 and EP50, with the percentage contributions of SOC ranging from 27 to 37%. In contrast, an opposite trend was found in EP47, EP49 and EP51, where SOC exhibited rapid increases, showing higher percentage contributions of 37-50%. It is worth noting that even under the influence of the same typhoon (i.e., EP46 vs. EP 47, EP49 vs, EP50), SOC exhibited distinct variations. These could be associated with the moving tracks of typhoon and its relative location with respect to Hong Kong.

The relationships of SOC with meteorological parameters and oxidants are investigated during the daytime and

nighttime episodic hours. Clear diurnal patterns with higher daytime concentrations were observed (Figure 7b), which could be associated with high emissions and strong atmospheric oxidation capacity during the daytime. SOC showed

440  a positive correlation with increased temperature in both daytime and nighttime episodic hours, with comparable coefficient ($r$ = 0.28-0.3, Figure S8a). SOC levels were comparable during the daytime episodic hours among different RH bins, while during nighttime, we observed the increase of SOC with RH raised from 60% to 90%, which might be associated with the aqueous phase reactions.
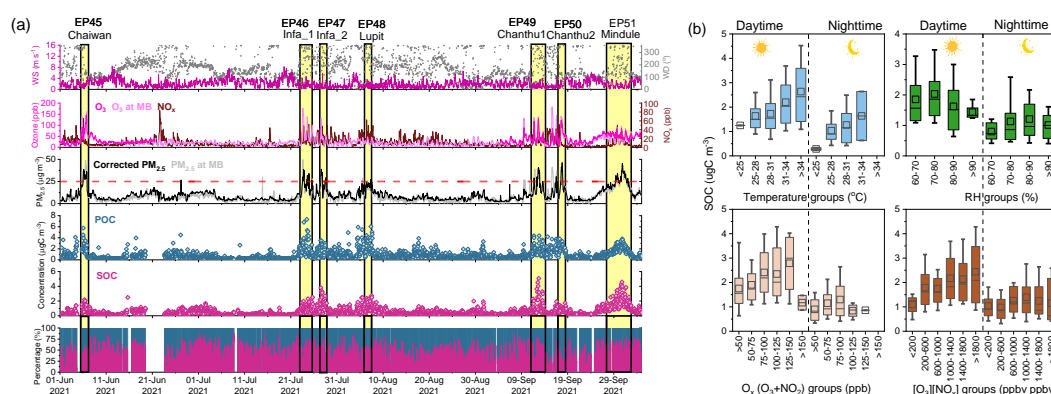
445  **Figure 7. SOC variation characteristics during typhoon episodes in summer 2021. (a) Time series of meteorological parameters (wind speed and direction), gaseous pollutants (O₃ and NOₓ), PM₂.₅ mass concentrations, POC and SOC levels and their relative percentage contributions, with the yellow shadow area marking individual episode periods of EP45-51. (b) Concentrations of SOC as a function of temperature, RH, Oₓ (O₃+NO₂) and NOₓ bins, with daytime and nighttime episode hours plotted separately.**

450  The responses of SOC to the oxidants are distinctive in the daytime and nighttime episodic hours. We observed the gradual increase of SOC when Oₓ levels <150 ppb during the daytime, but no clear trend was observed during the nighttime; this could be explained by the negligible photooxidation reactions. Previous study also observed better correlations of SOC with Oₓ in urban Hong Kong during the daytime (Zhou et al., 2014). SOC levels elevated more rapidly with the increase in NOₓ than O₃ in both daytime and nighttime episodic hours. The average levels of SOC

455  were double under conditions of NOₓ levels exceeding 20 ppb compared to the lowest NOₓ group, indicating that NOₓ played a more important role in SOC formation.

### 3.4.4 Winter haze episodes

In winter, PM₂.₅ episodes mainly occurred in December. During the winter episodes, northerly winds prevailed, and the wind speed generally exceeded 3 m s⁻¹ (Figure 8a). The city-wide PM₂.₅ showed a clear spatial gradient, with

460  higher levels observed at sites in the northwestern part of the city, followed by the central sites and eastern/southern sites (Figure S5). This spatial pattern is consistent with that wintertime air pollution in Hong Kong is frequently associated with regional transport coming from the north. Notably, the levels of PM₂.₅ were higher during the episodes in 2021 (EP10-13) than those in 2020 (EP62-65). This can be attributed to the increased intensity of anthropogenic emissions in 2021, as the pandemic restrictions in China were somewhat relaxed compared to 2020.
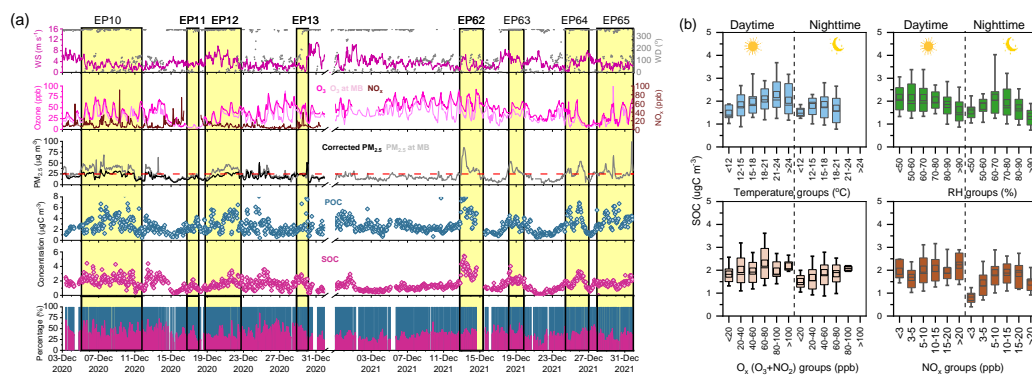
465

**Figure 8. SOC variation characteristics during haze episodes in winter 2020 and 2021. (a) Time series of meteorological parameters (wind speed and direction), gaseous pollutants (O$_3$ and NO$_x$), PM$_{2.5}$ mass concentrations, POC and SOC levels and their relative percentage contributions, with the yellow shadow area marking individual episodes (EP10-13 and EP62-65). (b) Concentrations of SOC as a function of temperature, RH, O$_x$ (O$_3$+NO$_2$) and NO$_x$ bins, with daytime and nighttime**
470 **episode hours plotted separately.**

Regarding POC and SOC, we observed enhancements of POC by 1.5-2 times during episodes compared to non-episode hours in the winter of 2020, however, SOC did not exhibit obvious elevation during these episodes. In the winter episodes of 2021, there was concurrent rapid increase in POC and SOC throughout the progression of the episodes. The highest SOC levels were observed in EP62, coinciding with the highest O$_3$ recorded during that episode

475 (Figure 8a). The percentage contributions of SOC varied among individual episodes, ranging from 29% to 41% in 2020 episodes and 32 to 38% in 2021 episodes.

Unlike the summer episodes, the winter episodes exhibited weak diurnal differences, in line with the regional source origin of the pollution, which persisted day and night. Positive correlations of SOC with temperature were only observed during daytime hours while the correlations were insignificant at night. Similar to summer typhoon episodes,

480 the SOC levels during the nighttime in winter initially increased with RH for the three lowest RH bins from < 50% to 70%, then decreased as RH further increased. Positive correlations were observed between SOC and O$_x$ levels during both daytime and nighttime, while the relationship with NO$_x$ was much weaker (Figure 8b). We observed better correlations of SOC with NO$_x$ during the nighttime ($r$: 0.24 vs. 0.12), highlighting a notable role of nighttime NO$_x$ chemistry in SOC formation. Previous studies have suggested that nighttime secondary formation is dependent on

485 NO$_3$ radical (Nah et al., 2016; Zhang et al., 2015). Feng et al. (2022) measured nocturnal NO$_3$ radical in Beijing and found that nighttime SOC formation was sensitive to the NO$_3$ radical, providing more direct evidence for the role of NO$_x$ through enhancing NO$_3$ radical during nighttime SOC formation. If we use [NO$_2$][O$_3$] as a rough indicator for the production of NO$_3$ radical (Wang et al., 2018), the observed good correlation between nighttime SOC with [NO$_2$][O$_3$] ($r = 0.36$) in this study implies that SOA formation pathways involving NO$_3$ radials were also active at our

490 site. Previous studies have indicated that NO$_3$ radials are highly reactive in the aqueous phase and can act as strong oxidants (Chameides, 1986; Wang et al., 2018). As AWC and acidity are the major factors for aqueous phase reactions (Jang et al., 2002; Jang et al., 2004), we investigated the relationship between SOC and AWC, as well as aerosol acidity. Table S3 tabulates the average AWC and [H$^+$] levels during episodic hours, calculated separately for daytime

and nighttime, showing higher AWC and acidity during the nighttime episodic hours. Figure S9a shows moderate
correlations of SOC with AWC and acidity during nighttime ($r = 0.30$ and $0.35$, respectively). The correlations during
daytime were much weaker ($r = 0.10$ and $0.11$, respectively), indicating that aqueous-phase reactions were negligible
during the day. The results, along with our analysis, indicate that acid-catalyzed aqueous-phase reactions involving
the $NO_3$ radical may represent notable formation pathways for nighttime SOC formation during winter haze episodes.

## 4 Conclusions

Organic carbonaceous aerosols play a significant role in formulating policies to control $PM_{2.5}$ pollution given their
increasing relative contribution to $PM_{2.5}$ in the ambient environment. Availability of POC and SOC from observation-
based measurements is crucial for refining atmospheric models and developing more effective measures to tackle
carbonaceous aerosol pollution and its associated impacts on climate change and public health. In this study, online
observation of major components of $PM_{2.5}$ for *ca*. one and a half years was conducted from 16 July 2020 to 31
December 2021 at a regional suburban site in Hong Kong. POC and SOC were differentiated using a novel Bayesian
inference approach, which yielded results that agree well with those derived from the elemental and organic tracer
based-PMF method. The model utilizing sulfate as a SOC tracer exhibited the lowest error and Bayesian Information
Criterion (BIC) values, making it a more suitable choice compared to other secondary inorganic ions, such as $NH_4^+$
and $NO_3^-$. We study the characteristics of aerosol carbonaceous components, including seasonal cycles, diurnal and
weekday/weekend patterns, and the influencing factors (i.e., meteorological parameters and oxidant levels)
contributing to SOC formation under varied PM pollution conditions. Positive correlation between SOC level and
ambient temperature was observed across different seasons. Substantially high SOC levels were associated with
increased $O_x$ concentration, especially in winter, highlighting the important role of photochemical reactions even under
weak radiation conditions. $NO_x$ was found to be significant in contributing to extensive SOC formation under pollution
conditions in summer.

A total of 65 city-wide $PM_{2.5}$ episodes were identified over the entire studied period, and the characteristics of POC
and SOC varied substantially among the episodes. An in-depth analysis of summer typhoon episodes and winter haze
episodes demonstrated the importance of meteorology and oxidant levels on the variations of SOC and the formation
processes. During summer typhoon episodes, the increased carbonaceous components were largely influenced by local
emissions resulting from impacts of the typhoons. Higher SOC levels were observed during the daytime, likely due to
enhanced oxidation reactions under high temperatures and stronger solar radiation. In winter haze episodes, the diurnal
difference was less obvious as the site was influenced by the continuous regional transport of air pollutants from
northern China. Notably, the nighttime aqueous-phase reactions involving the $NO_3$ radical were found to play an
important role in SOC formation during the episodic hours.

Overall, our findings demonstrate the diverse facilitating factors contributing to aerosol pollution episodes and
highlight the combined influences of meteorology and atmospheric oxidants on SOC formation. These results will be
valuable for modelling studies aiming to improve accuracy in evaluating SOC contributions and variations at both city
and regional scales. They will also aid the development of target-oriented strategies for air quality improvement.

*Data availability.* The hourly carbonaceous components and other chemical speciation data presented in this study are
530  available from the data repository maintained by HKUST: https://doi.org/10.14711/dataset/WYJQD0 (Yu and Wang,
2023).

*Supplement.* Figures S1-S9, and Tables S1-S3.

*Author contributions.* WANG Shan: Formal analysis, Investigation, Data curation, Visualization, Writing – original
draft, Writing – review & editing; Liao Kezheng: Methodology, Writing – review & editing; Yuk Ying Cheng, Zijing
535  Zhang, Qiongqiong WANG, and Hanzhe Chen: Measurement of other major components, Data validation. Jian Zhen
Yu: Conceptualization, Data curation, Project administration, Supervision, Writing – review & editing.

*Competing interests.* The contact author has declared that none of the authors has any competing interests.

*Disclaimer.* The content of this study does not necessarily reflect the views and policies of the HKSAR Government
nor does the mention of trade names or commercial products constitute an endorsement or recommendation of their
540  use.

*Acknowledgements.* We thank funding support from the Hong Kong Research Grants Council (R6011-18, 16305418,
and C5004-15E), and the Hong Kong University of Science and Technology (VPRDO19IP01).

**References**

Bian, Q., Alharbi, B., Shareef, M.M., Husain, T., Pasha, M.J., Atwood, S.A., Kreidenweis, S.M.: Sources of PM$_{2.5}$
545  carbonaceous aerosol in Riyadh, Saudi Arabia, Atmos. Chem. Phys., 18, 3969-3985. http://doi.org/10.5194/acp-18-3969-2018, 2018.

Blanchard, C.L., Hidy, G.M., Tanenbaum, S., Edgerton, E., Hartsell, B., Jansen, J.: Carbon in southeastern US aerosol
particles: Empirical estimates of secondary organic aerosol formation, Atmos. Environ., 42, 6710-6720.
http://doi.org/10.1016/j.atmosenv.2008.04.011, 2008.

550  Bond, T.C., Doherty, S.J., Fahey, D.W., Forster, P.M., Berntsen, T., et al.: Bounding the role of black carbon in the
climate system: A scientific assessment, J. Geophys. Res.-Atmos., 118, 5380-5552. http://doi.org/10.1002/jgrd.50171, 2013.

Hong Kong Environment Bureau: A Clean Air Plan for Hong Kong, 2013.

Hong Kong Environment Bureau: Clean Air Plan for Hong Kong 2035, 2021.

555  Cao, J., Lee, S.C., Ho, K.F., Zhang, X., Zou, S., et al.: Characteristics of carbonaceous aerosol in Pearl River Delta
Region, China during 2001 winter period, Atmos. Environ., 37, 1451-1460. http://doi.org/10.1016/s1352-2310(02)01002-6, 2003.

Castro, L.M., Pio, C.A., Harrison, R.M., Smith, D.J.T.: Carbonaceous aerosol in urban and rural European atmospheres:
estimation of secondary organic carbon concentrations, Atmos. Environ., 33, 2771-2781.
560  http://doi.org/10.1016/S1352-2310(98)00331-8, 1999.

Chameides, W.L.: Possible role of NO$_3$ in the nighttime chemistry of a cloud, J. Geophys. Res.-Atmos., 91, 5331-5337. http://doi.org/https://doi.org/10.1029/JD091iD05p05331, 1986.

Cheng, Y., Ma, Y., Hu, D.: Tracer-based source apportioning of atmospheric organic carbon and the influence of
anthropogenic emissions on secondary organic aerosol formation in Hong Kong, Atmos. Chem. Phys., 21, 10589-
565  10608. http://doi.org/10.5194/acp-21-10589-2021, 2021.

Chow, J.C., Watson, J.G., Crow, D., Lowenthal, D.H., Merrifield, T.: Comparison of IMPROVE and NIOSH carbon
measurements, Aerosol Sci. Technol., 34, 23-34. http://doi.org/10.1080/027868201300081923, 2001.

Chow, J.C., Watson, J.G., Lowenthal, D.H., Chen, L.W., Motallebi, N.: Black and organic carbon emission inventories: review and application to California, J. Air Waste Manag. Assoc., 60, 497-507. http://doi.org/10.3155/1047-3289.60.4.497, 2010.

Christian, T.J., Kleiss, B., Yokelson, R.J., Holzinger, R., Crutzen, P.J., et al.: Comprehensive laboratory measurements of biomass-burning emissions: 1. Emissions from Indonesian, African, and other fuels, J. Geophys. Res.-Atmos., 108. http://doi.org/10.1029/2003jd003704, 2003.

Day, M.C., Zhang, M., Pandis, S.N.: Evaluation of the ability of the EC tracer method to estimate secondary organic carbon, Atmos. Environ., 112, 317-325. http://doi.org/10.1016/j.atmosenv.2015.04.044, 2015.

Deng, W., Fang, Z., Wang, Z., Zhu, M., Zhang, Y., et al.: Primary emissions and secondary organic aerosol formation from in-use diesel vehicle exhaust: Comparison between idling and cruise mode, Sci. Total Environ., 699. http://doi.org/10.1016/j.scitotenv.2019.134357, 2020.

Ding, R., Li, J., Wang, S., Ren, F.: Decadal change of the spring dust storm in northwest China and the associated atmospheric circulation, Geophys. Res. Lett., 32. http://doi.org/10.1029/2004gl021561, 2005.

Ding, X., Wang, X.M., Zheng, M.: The influence of temperature and aerosol acidity on biogenic secondary organic aerosol tracers: Observations at a rural site in the central Pearl River Delta region, South China, Atmos. Environ., 45, 1303-1311. http://doi.org/10.1016/j.atmosenv.2010.11.057, 2011.

Donahue, N.M., Robinson, A.L., Pandis, S.N., Kroll, J.H., Worsnop, D.L.: Rethinking organic aerosols: Semivolatile emissions and photochemical aging, Geochim Cosmochim Ac, 73, A299-A299. 2009.

Fan, W., Chen, T., Zhu, Z., Zhang, H., Qiu, Y., Yin, D.: A review of secondary organic aerosols formation focusing on organosulfates and organic nitrates, J. Hazard. Mater., 430. http://doi.org/10.1016/j.jhazmat.2022.128406, 2022.

Feng, Z., Zheng, F., Liu, Y., Fan, X., Yan, C., et al.: Evolution of organic carbon during COVID-19 lockdown period: Possible contribution of nocturnal chemistry, Sci. Total Environ., 808. http://doi.org/10.1016/j.scitotenv.2021.152191, 2022.

Gentner, D.R., Jathar, S.H., Gordon, T.D., Bahreini, R., Day, D.A., et al.: Review of Urban Secondary Organic Aerosol Formation from Gasoline and Diesel Motor Vehicle Emissions, Environ. Sci. Technol., 51, 1074-1093. http://doi.org/10.1021/acs.est.6b04509, 2017.

Guo, S., Hu, M., Guo, Q., Zhang, X., Zheng, M., et al.: Primary sources and secondary formation of organic aerosols in Beijing, China, Environ. Sci. Technol., 46, 9846-9853. http://doi.org/10.1021/es2042564, 2012.

Hallquist, M., Wenger, J.C., Baltensperger, U., Rudich, Y., Simpson, D., et al.: The formation, properties and impact of secondary organic aerosol: current and emerging issues, Atmos. Chem. Phys., 9, 5155-5236. http://doi.org/10.5194/acp-9-5155-2009, 2009.

Hu, D., Bian, Q., Lau, A.K.H., Yu, J.Z.: Source apportioning of primary and secondary organic carbon in summer $PM_{2.5}$ in Hong Kong using positive matrix factorization of secondary and primary organic tracer data, J. Geophys. Res.-Atmos., 115. http://doi.org/10.1029/2009jd012498, 2010.

Hu, D., Bian, Q., Li, T.W.Y., Lau, A.K.H., Yu, J.Z.: Contributions of isoprene, monoterpenes, β-caryophyllene, and toluene to secondary organic aerosols in Hong Kong during the summer of 2006, J. Geophys. Res.-Atmos., 113. http://doi.org/10.1029/2008jd010437, 2008.

Huang, R., Zhang, Y., Bozzetti, C., Ho, K.F., Cao, J., et al.: High secondary aerosol contribution to particulate pollution during haze events in China, Nature, 514, 218-222. http://doi.org/10.1038/nature13774, 2014.

Jaeckels, J.M., Bae, M.S., Schauer, J.J.: Positive matrix factorization (PMF) analysis of molecular marker measurements to quantify the sources of organic aerosols, Environ. Sci. Technol., 41, 5763-5769. http://doi.org/10.1021/es062536b, 2007.

Jang, M., Czoschke, N.M., Lee, S., Kamens, R.M.: Heterogeneous atmospheric aerosol production by acid-catalyzed particle-phase reactions, Science, 298, 814-817. http://doi.org/10.1126/science.1075798, 2002.

Jang, M., Czoschke, N.M., Northcross, A.L.: Atmospheric organic aerosol production by heterogeneous acid-catalyzed reactions, Chemphyschem, 5, 1647-1661. http://doi.org/10.1002/cphc.200301077, 2004.

Jathar, S.H., Miracolo, M.A., Tkacik, D.S., Donahue, N.M., Adams, P.J., Robinson, A.L.: Secondary Organic Aerosol Formation from Photo-Oxidation of Unburned Fuel: Experimental Results and Implications for Aerosol Formation from Combustion Emissions, Environ. Sci. Technol., 47, 12886-12893. http://doi.org/10.1021/es403445q, 2013.

Ke, L., Liu, W., Wang, Y., Russell, A.G., Edgerton, E.S., Zheng, M.: Comparison of $PM_{2.5}$ source apportionment using positive matrix factorization and molecular marker-based chemical mass balance, Sci. Total Environ., 394, 290-302.

http://doi.org/10.1016/j.scitotenv.2008.01.030, 2008.

620   Kim, W., Lee, H., Kim, J., Jeong, U., Kweon, J.: Estimation of seasonal diurnal variations in primary and secondary organic carbon concentrations in the urban atmosphere: EC tracer and multiple regression approaches, Atmos. Environ., 56, 101-108. http://doi.org/10.1016/j.atmosenv.2012.03.076, 2012.

Kleindienst, T.E., Jaoui, M., Lewandowski, M., Offenberg, J.H., Docherty, K.S.: The formation of SOA and chemical tracer compounds from the photooxidation of naphthalene and its methyl analogs in the presence and absence of
625   nitrogen oxides, Atmos. Chem. Phys., 12, 8711-8726. http://doi.org/10.5194/acp-12-8711-2012, 2012.

Kleindienst, T.E., Jaoui, M., Lewandowski, M., Offenberg, J.H., Lewis, C.W., Bhave, P.V., Edney, E.O.: Estimates of the contributions of biogenic and anthropogenic hydrocarbons to secondary organic aerosol at a southeastern US location, Atmos. Environ., 41, 8288-8300. http://doi.org/10.1016/j.atmosenv.2007.06.045, 2007.

Kley, D., Geiss, H., Mohnen, V.A.: Tropospheric Ozone at Elevated Sites and Precursor Emissions in the United-States
630   and Europe, Atmos. Environ., 28, 149-158. http://doi.org/10.1016/1352-2310(94)90030-2, 1994.

Klingshirn, C.D., West, Z.J., DeWitt, M.J., Higgins, A., Graham, J., Corporan, E.: Quantification of elemental and total carbon in combustion particulate matter using thermal-oxidative analysis, J. Air Waste Manag. Assoc., 69, 1003-1013. http://doi.org/10.1080/10962247.2019.1630025, 2019.

Kroll, J.H., Donahue, N.M., Jimenez, J.L., Kessler, S.H., Canagaratna, M.R., et al.: Carbon oxidation state as a metric
635   for describing the chemistry of atmospheric organic aerosol, Nat. Chem., 3, 133-139. http://doi.org/10.1038/Nchem.948, 2011.

Li, J., Han, Z., Li, J., Liu, R., Wu, Y., Liang, L., Zhang, R.: The formation and evolution of secondary organic aerosol during haze events in Beijing in wintertime, Sci. Total Environ., 703, 134937. http://doi.org/10.1016/j.scitotenv.2019.134937, 2020.

640   Li, J., Yu, X., Li, Q., Wang, S., Cheng, Y.Y., Yu, J.Z.: Online measurement of aerosol inorganic and organic nitrogen based on thermal evolution and chemiluminescent detection, Atmos. Environ., 271. http://doi.org/10.1016/j.atmosenv.2021.118905, 2022.

Li, Y., Yu, J.Z., Ho, S.S.H., Schauer, J.J., Yuan, Z., Lau, A.K.H., Louie, P.K.K.: Chemical characteristics and source apportionment of fine particulate organic carbon in Hong Kong during high particulate matter episodes in winter 2003,
645   Atmos. Res., 120-121, 88-98. http://doi.org/10.1016/j.atmosres.2012.08.005, 2013.

Liao, K., Wang, Q., Wang, S., Yu, J.Z.: Bayesian Inference Approach to Quantify Primary and Secondary Organic Carbon in Fine Particulate Matter Using Major Species Measurements, Environ. Sci. Technol., 57, 5169-5179. http://doi.org/10.1021/acs.est.2c09412, 2023.

Nah, T., Sanchez, J., Boyd, C.M., Ng, N.L.: Photochemical Aging of alpha-pinene and beta-pinene Secondary Organic
650   Aerosol formed from Nitrate Radical Oxidation, Environ. Sci. Technol., 50, 222-231. http://doi.org/10.1021/acs.est.5b04594, 2016.

Nel, A.: Air pollution-related illness: Effects of particles, Science, 308, 804-806. http://doi.org/10.1126/science.1108752, 2005.

Notario, A., Bravo, I., Adame, J.A., Díaz-de-Mera, Y., Aranda, A., Rodríguez, A., Rodríguez, D.: Variability of
655   oxidants ($O_X=O_3+NO_2$), and preliminary study on ambient levels of ultrafine particles and VOCs, in an important ecological area in Spain, Atmos. Res., 128, 35-45. http://doi.org/10.1016/j.atmosres.2013.03.008, 2013.

Pachon, J.E., Balachandran, S., Hu, Y.T., Weber, R.J., Mulholland, J.A., Russell, A.G.: Comparison of SOC estimates and uncertainties from aerosol chemical composition and gas phase data in Atlanta, Atmos. Environ., 44, 3907-3914. http://doi.org/10.1016/j.atmosenv.2010.07.017, 2010.

660   Roberts, J.M.: The Atmospheric Chemistry of Organic Nitrates, Atmos. Environ., 24, 243-287. http://doi.org/10.1016/0960-1686(90)90108-Y, 1990.

Schauer, J.J., Cass, G.R.: Source apportionment of wintertime gas-phase and particle-phase air pollutants using organic compounds as tracers, Environ. Sci. Technol., 34, 1821-1832. http://doi.org/10.1021/es981312t, 2000.

Seinfeld, J.H., Pandis, S.N.: Atmospheric Chemistry and Physics: From Air Pollution to Climate Change. Wiley, New
665   York, 1998.

Shi, G., Tian, Y., Zhang, Y., Ye, W., Li, X., et al.: Estimation of the concentrations of primary and secondary organic carbon in ambient particulate matter: Application of the CMB-Iteration method, Atmos. Environ., 45, 5692-5698. http://doi.org/10.1016/j.atmosenv.2011.07.031, 2011.

So, K.L., Wang, T.: On the local and regional influence on ground-level ozone concentrations in Hong Kong, Environ

670    Pollut, 123, 307-317. http://doi.org/10.1016/s0269-7491(02)00370-6, 2003.

Stone, E.A., Zhou, J.B., Snyder, D.C., Rutter, A.P., Mieritz, M., Schauer, J.J.: A Comparison of Summertime Secondary Organic Aerosol Source Contributions at Contrasting Urban Locations, Environ. Sci. Technol., 43, 3448-3454. http://doi.org/10.1021/es8025209, 2009.

Svendby, T.M., Lazaridis, M., Tørseth, K.: Temperature dependent secondary organic aerosol formation from terpenes
675    and aromatics, J. Atmos. Chem., 59, 25-46. http://doi.org/10.1007/s10874-007-9093-7, 2008.

Turpin, B.J., Huntzicker, J.J.: Secondary Formation of Organic Aerosol in the Los-Angeles Basin - a Descriptive Analysis of Organic and Elemental Carbon Concentrations, Atmos. Environ., 25, 207-215. http://doi.org/10.1016/0960-1686(91)90291-E, 1991.

Wang, H., Lu, K., Guo, S., Wu, Z., Shang, D., et al.: Efficient $N_2O_5$ uptake and $NO_3$ oxidation in the outflow of urban
680    Beijing, Atmos. Chem. Phys., 18, 9705-9721. http://doi.org/10.5194/acp-18-9705-2018, 2018.

Wang, M., Duan, Y., Xu, W., Wang, Q., Zhang, Z., et al.: Measurement report: Characterisation and sources of the secondary organic carbon in a Chinese megacity over 5 years from 2016 to 2020, Atmos. Chem. Phys., 22, 12789-12802. http://doi.org/10.5194/acp-22-12789-2022, 2022a.

Wang, Q., He, X., Huang, X.H.H., Griffith, S.M., Feng, Y., et al.: Impact of Secondary Organic Aerosol Tracers on
685    Tracer-Based Source Apportionment of Organic Carbon and $PM_{2.5}$: A Case Study in the Pearl River Delta, China, ACS Earth Sp. Chem., 1, 562-571. http://doi.org/10.1021/acsearthspacechem.7b00088, 2017.

Wang, Q., Wang, S., Cheng, Y.Y., Chen, H., Zhang, Z., et al.: Chemical evolution of secondary organic aerosol tracers during high-$PM_{2.5}$ episodes at a suburban site in Hong Kong over 4 months of continuous measurement, Atmos. Chem. Phys., 22, 11239-11253. http://doi.org/10.5194/acp-22-11239-2022, 2022b.

690    Wang, S., Wang, Q., Cheng, Y.Y., Chen, H., Zhang, Z., et al.: Molecular and Elemental tracers-based Receptor modeling of $PM_{2.5}$ in Suburban Hong Kong with Hourly Time-scale Air Quality Considerations, Under review, 2023a.

Wang, S., Wang, Q., Cheng, Y.Y., Chen, H., Zhang, Z., et al.: Hourly time-scale characterization of secondary organic aerosols and source apportionment of $PM_{2.5}$ and organic carbon during haze, ozone and dust episodes at suburban Hong Kong, under preparation, 2023b.

695    Wang, S., Wang, Q., Zhu, S., Zhou, M., Qiao, L., et al.: Hourly organic tracers-based source apportionment of $PM_{2.5}$ before and during the Covid-19 lockdown in suburban Shanghai, China: Insights into regional transport influences and response to urban emission reductions, Atmos. Environ., 289, 119308. http://doi.org/10.1016/j.atmosenv.2022.119308, 2022c.

Wang, X., Dong, Z., Zhang, J., Liu, L.: Modern dust storms in China: an overview, J. Arid Environ., 58, 559-574.
700    http://doi.org/10.1016/j.jaridenv.2003.11.009, 2004.

Wang, Z., Wang, T., Guo, J., Gao, R., Xue, L., et al.: Formation of secondary organic carbon and cloud impact on carbonaceous aerosols at Mount Tai, North China, Atmos. Environ., 46, 516-527. http://doi.org/10.1016/j.atmosenv.2011.08.019, 2012.

Wong, Y.K., Liu, K.M., Yeung, C., Leung, K.K.M., Yu, J.Z.: Measurement report: Characterization and source
705    apportionment of coarse particulate matter in Hong Kong: insights into the constituents of unidentified mass and source origins in a coastal city in southern China, Atmos. Chem. Phys., 22, 5017-5031. http://doi.org/10.5194/acp-22-5017-2022, 2022.

Wu, C., Wu, D., Yu, J.Z.: Estimation and Uncertainty Analysis of Secondary Organic Carbon Using 1 Year of Hourly Organic and Elemental Carbon Data, J. Geophys. Res.-Atmos., 124, 2774-2795. http://doi.org/10.1029/2018jd029290,
710    2019.

Wu, C., Yu, J.Z.: Determination of primary combustion source organic carbon-to-elemental carbon (OC / EC) ratio using ambient OC and EC measurements: secondary OC-EC correlation minimization method, Atmos. Chem. Phys., 16, 5453-5465. http://doi.org/10.5194/acp-16-5453-2016, 2016.

Yao, L., Huo, J., Wang, D., Fu, Q., Sun, W., Li, Q., Chen, J.: Online measurement of carbonaceous aerosols in suburban
715    Shanghai during winter over a three-year period: Temporal variations, meteorological effects, and sources, Atmos. Environ., 226. http://doi.org/10.1016/j.atmosenv.2020.117408, 2020.

Yu, J.Z.: Chemical Characterization of Water Soluble Organic Compounds in Particulate Matters in Hong Kong. Hong Kong Environmental Protection Department, 2002.

Yuan, Z., Yu, J.Z., Lau, A.K.H., Louie, P.K.K., Fung, J.C.H.: Application of positive matrix factorization in estimating
720    aerosol secondary organic carbon in Hong Kong and its relationship with secondary sulfate, Atmos. Chem. Phys., 6,

25-34. http://doi.org/10.5194/acp-6-25-2006, 2006.

Zhang, R., Wang, G., Guo, S., Zarnora, M.L., Ying, Q., et al.: Formation of Urban Fine Particulate Matter, Chem. Rev., 115, 3803-3855. http://doi.org/10.1021/acs.chemrev.5b00067, 2015.

725    Zhang, Y., Mao, H., Ding, A., Zhou, D., Fu, C.: Impact of synoptic weather patterns on spatio-temporal variation in surface $O_3$ levels in Hong Kong during 1999–2011, Atmos. Environ., 73, 41-50. http://doi.org/10.1016/j.atmosenv.2013.02.047, 2013.

Zhao, Y., Hu, M., Slanina, S., Zhang, Y.: Chemical compositions of fine particulate organic matter emitted from Chinese cooking, Environ. Sci. Technol., 41, 99-105. http://doi.org/10.1021/es0614518, 2007.

730    Zhou, S., Wang, T., Wang, Z., Li, W., Xu, Z., et al.: Photochemical evolution of organic aerosols observed in urban plumes from Hong Kong and the Pearl River Delta of China, Atmos. Environ., 88, 219-229. http://doi.org/10.1016/j.atmosenv.2014.01.032, 2014.

Zhu, S., Wang, Q., Qiao, L., Zhou, M., Wang, S., et al.: Tracer-based characterization of source variations of $PM_{2.5}$ and organic carbon in Shanghai influenced by the COVID-19 lockdown, Faraday Discuss., 226, 112-137. http://doi.org/10.1039/d0fd00091d, 2021.

735